Water Research 260 (2024) 121854

Contents lists available at ScienceDirect

Water Research

journal homepage: www.elsevier.com/locate/watres

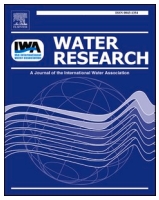

Hydrographic proxies for submarine groundwater discharge in the Jiulong River estuary and global perspectives

Moge Du [a], Shilei Jin [a], Siqi Wu [a], Yanzhen Liao [b,c], Guizhi Wang [a,d,*]

[a] State Key Laboratory of Marine Environmental Science and College of Ocean and Earth Sciences, Xiamen University, Xiamen, 361102, China
[b] Fujian Provincial Key Laboratory of Disaster Weather, Fuzhou, China
[c] Meteorological Administration of Zhangzhou in China, Zhangzhou, China
[d] National Observation and Research Station for the Taiwan Strait Marine Ecosystem, Xiamen University, Zhangzhou, China

ARTICLE INFO

Keywords:
Submarine groundwater discharge
Jiulong River estuary
^{226}Ra
^{228}Ra
Hydrographic proxies

ABSTRACT

Submarine groundwater discharge (SGD) significantly impacts most coastal waters. However, its quantification, depending on chemical tracers/proxies, limits its parameterization in numerical models. This study explored the hydrographic proxies of SGD in the Jiulong River estuary (JRE) using ^{226}Ra and ^{228}Ra as SGD tracers. Our results showed significant monthly fluctuations in the flux of SGD, with a peak in June and a minimum in April. On average, the flux of SGD was equivalent to 10 ± 1.67 % of the concurrent river discharge, with the area-normalized rate of 0.007 ± 0.017 to 0.13 ± 0.04 m/day. Positive SGD response to river discharge implies a connection with the surface runoff of the shallow aquifers. Furthermore, the flux of SGD presented a significant negative correlation with the return flow factor and flushing time of the estuary. The radium activities in the estuary were positively correlated with water depth, indicating that SGD was not driven by tidal pumping. Instead, physical mixing in low to middle salinity regions predominated such behavior of radium. Our results indicate that river discharge, flushing time and return flow factor may serve as hydrographic proxies of SGD in the JRE and potentially be applicable in parameterization of SGD in numerical models in similar coastal ecosystems. Globally, a positive correlation between SGD flux and river discharge emphasizes the latter as a general proxy in estuaries.

1. Introduction

An estuary is a hydrological environment where not only river water and seawater meet but also submarine groundwater (SGD) discharges. SGD is described as any and all flow of water on continental margins from the seabed to the coastal ocean, regardless of fluid composition or driving force (Burnett and Dulaiova, 2003). SGD can be composed of fresh submarine groundwater (FSGD), driven by a hydraulic gradient, and saline recirculated submarine groundwater (RSGD), driven by tidal pumping or wave setup (Santos et al., 2012). RSGD usually accounts for the majority of the total SGD on regional or global scales (Kim et al., 2003; Kwon et al., 2014; Luijendijk et al., 2020; Zhang et al., 2024). Associated with SGD, a subterranean estuary (STE) is defined as a coastal aquifer that performs as a connecting channel and mixing area of groundwater and seawater (Duque et al., 2020; Moore, 1999). The reactions resulting from mixing of waters from different origins in the STE exert an important control on the unique biogeochemical signature of SGD.

Subsequently, significant biogeochemical effects of SGD on element budgets and biogeochemical processes have been widely demonstrated in various coastal ecosystems around the globe. With nutrient fluxes comparable to riverine fluxes in quite a few ecosystems (Santos et al., 2021), SGD would fuel considerable primary production in the receiving coastal waters. Moreover, SGD, by and large, has an N:P ratio much higher than the Redfield ratio of 16:1 and is a crucial source of N in coastal ecosystems (Santos et al., 2021). In some STEs with rapid organic matter degradation, the inorganic carbon pool in the surface estuaries is greatly influenced by SGD. For example, in the Pearl River estuary, SGD is revealed as a potential net source of atmospheric CO_2 with a flux of 1.46×10^9 g C/day, which is ~50 % equivalent to the riverine flux (Wang et al., 2021). Moreover, SGD could alter the nearshore dissolved organic carbon (DOC) reactivity and bring excess DOC equivalent to 0.5 - 9 % of the offshore DOC concentration along the Santa Barbara coastline (Goodridge, 2018). In Sydney Harbor, the SGD-delivered DOC flux is greater than the riverine flux by a factor of two (Escobar Correa,

* Corresponding author.
E-mail address: gzhwang@xmu.edu.cn (G. Wang).

https://doi.org/10.1016/j.watres.2024.121854
Received 1 March 2024; Received in revised form 21 May 2024; Accepted 28 May 2024
Available online 31 May 2024

2021). The biogeochemical importance of SGD in these coastal systems necessitates its inclusion in any coastal biogeochemical model. However, due to great heterogeneity of aquifers such as topography (Luijendijk et al., 2020; Michael et al., 2013) and permeability (Kim et al., 2008; Santos et al., 2009), the flux of SGD is often highly spatially variable with various regulating factors. Furthermore, the temporal variation in the flux of SGD has been observed to be greater than its spatial variation in the Bay of Bengal (Debnath and Mukherjee, 2016). Hydrodynamic models have applied geographic structures, including hydraulic conductivity, aquifer thickness, topographic slope, and geochemical tracers to simulate the flux of SGD (Luijendijk et al., 2020; Yu et al., 2022). However, determination of general SGD proxies that can be routinely measured is lacking so that parameterization of the flux of SGD is usually an overlooked piece in coastal physical and biogeochemical models.

As an attempt to fill in the missing piece, we zoomed in a specific coastal ecosystem, the Jiulong River estuary (JRE) using long-lived radium isotopes, ^{226}Ra (half-life of 1600 years) and ^{228}Ra (half-life of 5.75 years), as SGD tracers. These isotopes have been broadly applied in tracing SGD due to their relatively high signals in coastal aquifers than in surface waters (Boehm et al., 2006; Rodellas et al., 2017). The flux of SGD in the JRE is revealed based on the mass balance of these tracers to be the highest in summer and the lowest in winter, with a seasonal pattern the same as that of the river discharge (Wang et al., 2015), indicating some relation between the river discharge and SGD. To investigate whether the river discharge can be a proxy of the flux of SGD in the JRE, and whether there are other physical factors such as tidal pumping driving the variation in the flux of SGD, an investigation with a higher temporal resolution is needed. Thus, in this study we conducted mapping surveys of ^{226}Ra and ^{228}Ra every two months for a year and a diel-cycle investigation every hour in the JRE. With a compilation of global data, we propose that river discharge and flushing time be potential hydrographic proxies of SGD in prediction and numerical simulation.

2. Materials and methods

2.1. Study area

The Jiulong River is the second largest river in Fujian Province, China, with three tributaries, the North Stream (the main stream), the West Stream, and the South Stream, flowing into Xiamen Bay and further into the Taiwan Strait (Fig. 1a). The annual average river discharge is 1.47×10^{10} m^3/y (Zhang et al., 2022). The JRE is located in the Longhai alluvial plain and is dominated by regular semidiurnal tides with an average tidal range of 3.9 m. The surface sediments (from 5 - 10 cm below the seabed) are mainly composed of clayey silts and coarse medium sands (Zuo et al., 2016).

Mapping cruises were carried out in February, April, June, August, October, and December of 2014 in the JRE along the main water channel (Fig. 1b). In addition, a diel-cycle investigation was conducted every hour at Station A8 from 9:40 a.m. on November 24, 2011 to evaluate the tidal effect. The weekly average river discharge before each investigation ranged from 2.89×10^7 to 6.56×10^7 m^3/day, with the maximum in June and the minimum in December (Fig. 2). The monthly precipitation in the JRE varies from 0 to 387.4 mm in 2014, with the maximum in June and the rainy season from May to August, during which the precipitation (1080.9 mm) accounted for 80 % of the annual rainfall. We took Stations A4, A5, and A6 in the upper estuary as the river end-member, Stations A7, A8, A9, A9–1, and JY0 (if sampled) as the estuary domain, and Stations JY1, JY2, JY3, and KM2 (if sampled) as the ocean end-member. The domestic well waters, taken as the SGD end-member and sampled around the JRE in the previous study (Wang et al., 2015), are presented (Fig. 1b). Among these SGD end-members, the stations with relatively high salinity, GW6-a (S = 6.5) and GW11 (S = 15), were termed as the range of the SGD end-member for the conservative estimations of minimum total SGD. Since the spatial variation in the chemical composition of the SGD end-member was much

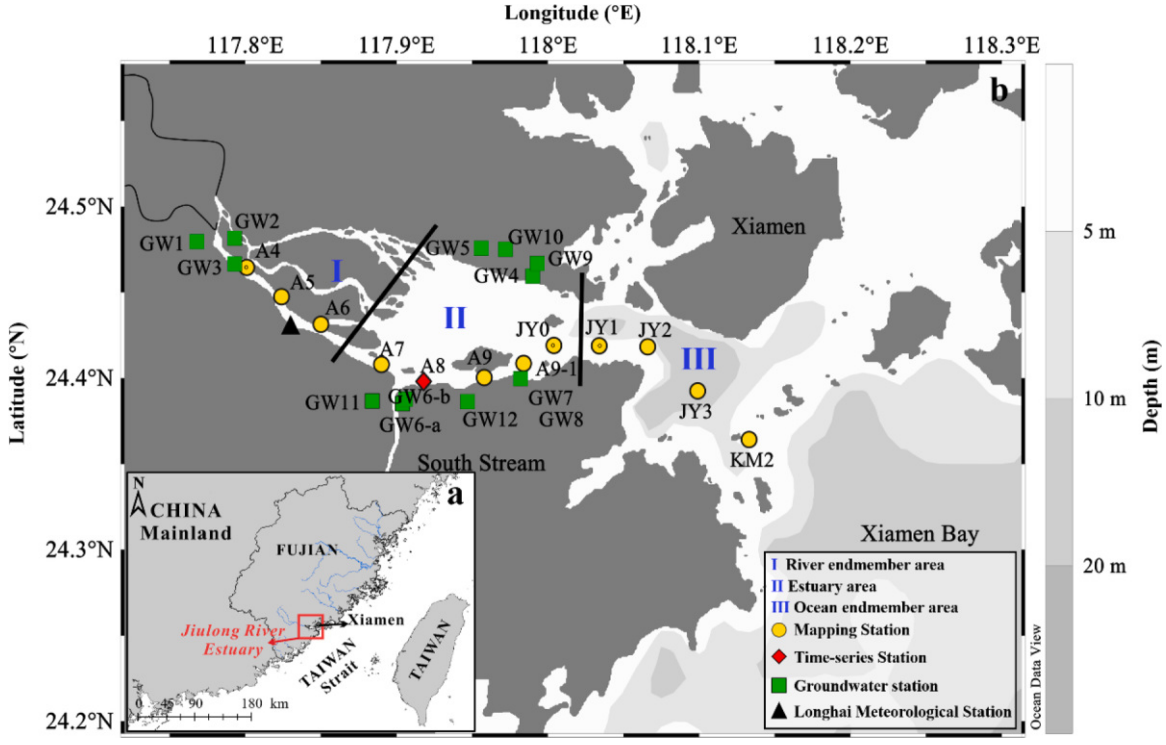

Fig. 1. Study area (a) and sampling stations in the Jiulong River estuary (b). The mapping area is divided to Area I: the river end-member area, including Stations A4, A5, and A6, Area II: the estuary area, including Stations A7, A8, A9, A9–1, and JY0, and Area III: the ocean end-member area, including Stations JY1, JY2, JY3, and KM2.

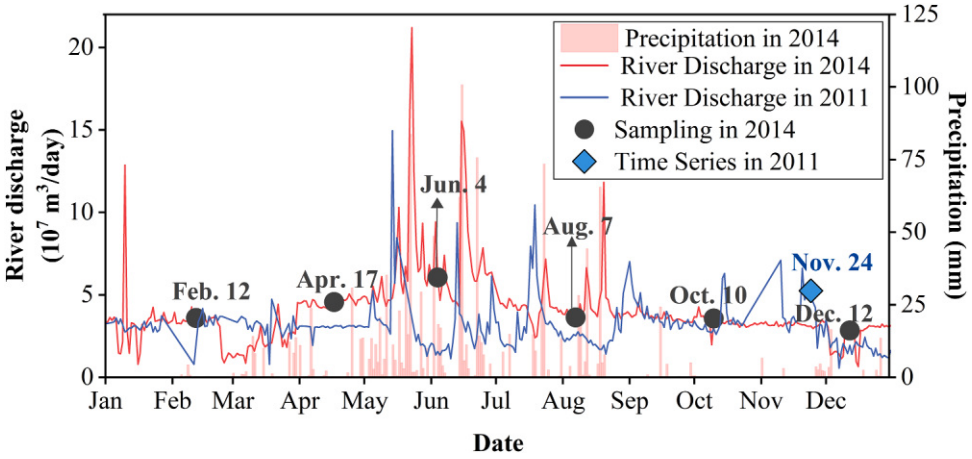

Fig. 2. Daily Jiulong River discharges in 2011 and 2014 and daily precipitation in 2014, and the river discharge is the sum of the records at hydrological stations Punan (24.64 °N, 117.67 °E) and Zhengdian (24.57 °N, 117.53 °E) available on the National Water and Rain Information website: http://xxfb.mwr.cn/sq_djdh.html. The precipitation data in 2014 were collected at Longhai meteorological station (24.40 °N, 117.83 °E) available on the website: http://www.weather.com.cn/.

greater than its seasonal variation (Wang et al., 2015), its temporal variability was ignored in our calculations.

2.2. Sampling and measurements

We collected 20 L surface water samples using a plastic barrel at the time-series station and 30 L at the mapping stations and filtered them through a polypropylene cartridge followed by MnO_2-coated fibers (Mn-fibers) to extract dissolved radium. The salinity and temperature of these samples were measured with a WTW multi 340i probe (Geotech) with measurement errors of 0.1 for salinity and 0.1 °C for temperature. The salinity reported is in Practical Salinity Scale. Total suspended matter (TSM) was collected on a pre-weighed 47-mm-diameter glass fiber filter (pore size of 0.7 μm, GF/F) and measured gravimetrically as the difference between the pre-weighed and filtered GF/F filter after oven-drying to a constant weight. The Mn-fibers were desalted with reverse osmosis (RO) water and dried afterwards until the weight ratio of water to fiber was about 1:1. The activities of ^{226}Ra and ^{228}Ra were measured using a high purity germanium gamma spectrometer (GCW4022, CANBERRA) after being co-precipitated with barium sulfate. The measurement error was within 3.80% for ^{226}Ra and 5.83% for ^{228}Ra. All the measurement data are listed in the Supporting Information Dataset 1.

3. Calculations

3.1. Estimation of the return flow factor

End-member mixing model is a widely used technique for quantifying the proportions of different source components, particularly in complex hydrological environments such as estuaries with multiple water sources (Moore, 2003; 2006). The model is based on mass balance of conservative parameters. In this study, the long-lived radium and salinity in the estuary are conservative and affected by three water masses, the ocean water, the river water, and SGD. Each water mass has a characteristic salinity and radium activities, thus the proportion of each water mass in the estuary can be calculated using the following equations:

$$\begin{cases} f_O + f_R + f_{SGD} = 1 \\ S_O \cdot f_O + S_R \cdot f_R + S_{SGD} \cdot f_{SGD} = S_E \\ {}^{i}Ra_O \cdot f_O + {}^{i}Ra_R \cdot f_R + {}^{i}Ra_{SGD} \cdot f_{SGD} = {}^{i}Ra_E \end{cases} \quad (1)$$

where f is the fraction of each water mass, S represents salinity, the subscripts, O, R, E, and SGD, represent the ocean water, river water, the estuary water, and SGD, respectively, and ${}^{i}Ra$ represents the activity of dissolved radium isotope corrected by particle desorption (i = 226 or 228) (The correction details are provided in the Appendix A1). The fraction of the ocean water, f_O, was taken as the return flow factor in the estuary, which denotes as b.

3.2. Determination of the flushing time

Flushing time (T_f) is an integrative parameter referring to the time required to replace the water in the estuary with the river discharge and tides. The tidal prism model, as described by Sanford (1992), offers a robust approach to calculating flushing time. This model relies on the volume of water exchanged during a tidal cycle (the tidal prism) to determine the rate at which a water body is flushed. By comparing the tidal prism with the total volume of the water body, we can estimate the flushing time, providing a quantitative basis for understanding SGD. The calculation is as follows,

$$T_f = \frac{A_E \cdot H \cdot T}{(1-b) \cdot V_P + F_R \cdot T} \quad (2)$$

where A_E represents the area of the estuary defined in this and previous studies (Wang et al., 2015), 7.11×10^7 m^2, H is the average water depth of the estuary, V_P is the volume of the tidal prism, taken as 3.3×10^8 m^3 (Jiang and Wai, 2005), F_R is the river discharge, and T is the tidal period, 12 h and 40 min.

3.3. Estimation of the Flux of SGD

For mapping observations, we applied a box model to calculate the flux of SGD. The box model is based on the mass balance of ^{226}Ra and ^{228}Ra under the assumption of steady state (Burnett et al., 2006; Crusius et al., 2005). In this study, we took the estuary domain as a box. The sources of Ra in the box consisted of the river input (including dissolved radium and what was desorbed from suspended particles), SGD, and sediment diffusion. The loss term of Ra was mainly mixing with the ocean. Even considering the longest flushing time (2.37 days) based on previous estimation (Wang et al., 2015), the decay loss of ^{226}Ra and ^{228}Ra was less than 1 ‰ (0.0028 ‰ and 0.76 ‰, respectively), negligible compared to other sources and sinks.

Under the assumption of steady state, the input of radium into the estuary was balanced by its loss. The mass balance of radium was set up as

$$F_R \cdot {}^{i}Ra_R + {}^{i}F_{sed} \cdot A_E + F_R \cdot {}^{i}Ra_d \cdot C_{TSM} + F_{SGD} \cdot {}^{i}Ra_{SGD} = A_E \cdot H \cdot \left({}^{i}Ra_E - b \cdot {}^{i}Ra_O \right) \cdot \frac{1}{T_f} \quad (3)$$

where ${}^{i}F_{sed}$ represents the radium diffusion flux from sediments, we adopted the values of 0.45 dpm/m^2/day for ${}^{226}F_{sed}$, and 25 dpm/m^2/day for ${}^{228}F_{sed}$ in the northern South China Sea (Liu et al., 2012). C_{TSM} is the concentration of total suspended matter at Station A6, which is the nearest station to the estuary. This concentration could represent the riverine particle transported into the estuary. ${}^{i}Ra_d$ is the activity of ^{226}Ra or ^{228}Ra desorbed from suspended particles (see estimations in the Appendix A1), and F represents fluxes from each source. The resuspension terms are considered by correcting the ${}^{i}Ra_E$ with the activity induced by resuspended TSM. When all the other parameters were known as listed in the Supporting Information Dataset 2, the flux of SGD was estimated from Eq. (3).

For time series observations, we calculated the SGD seepage rate based on a non-steady state procedure (Chen et al., 2014) as follows:

The excess Ra inventory, *I(t)*, was calculate over each measurement interval.

$$I(t) = \left[{}^{i}Ra_{total}(t) - {}^{i}Ra_{off}(t) \right] \times h(t) \quad (4)$$

where superscript i denotes 226 or 228 and *h(t)* denotes the water depth at time *t*. The subscript 'total' denotes the measured radium activity at time *t* and the 'off' here denotes the lowest measured radium activity of the time series data. Then, the inventory was corrected for tidal effect, in which during the flood tide

$$Corrected\ I(t) = I(t) - \left[h(t) - h(t-1) \times {}^{i}Ra_{off}(t) \right] \quad (5)$$

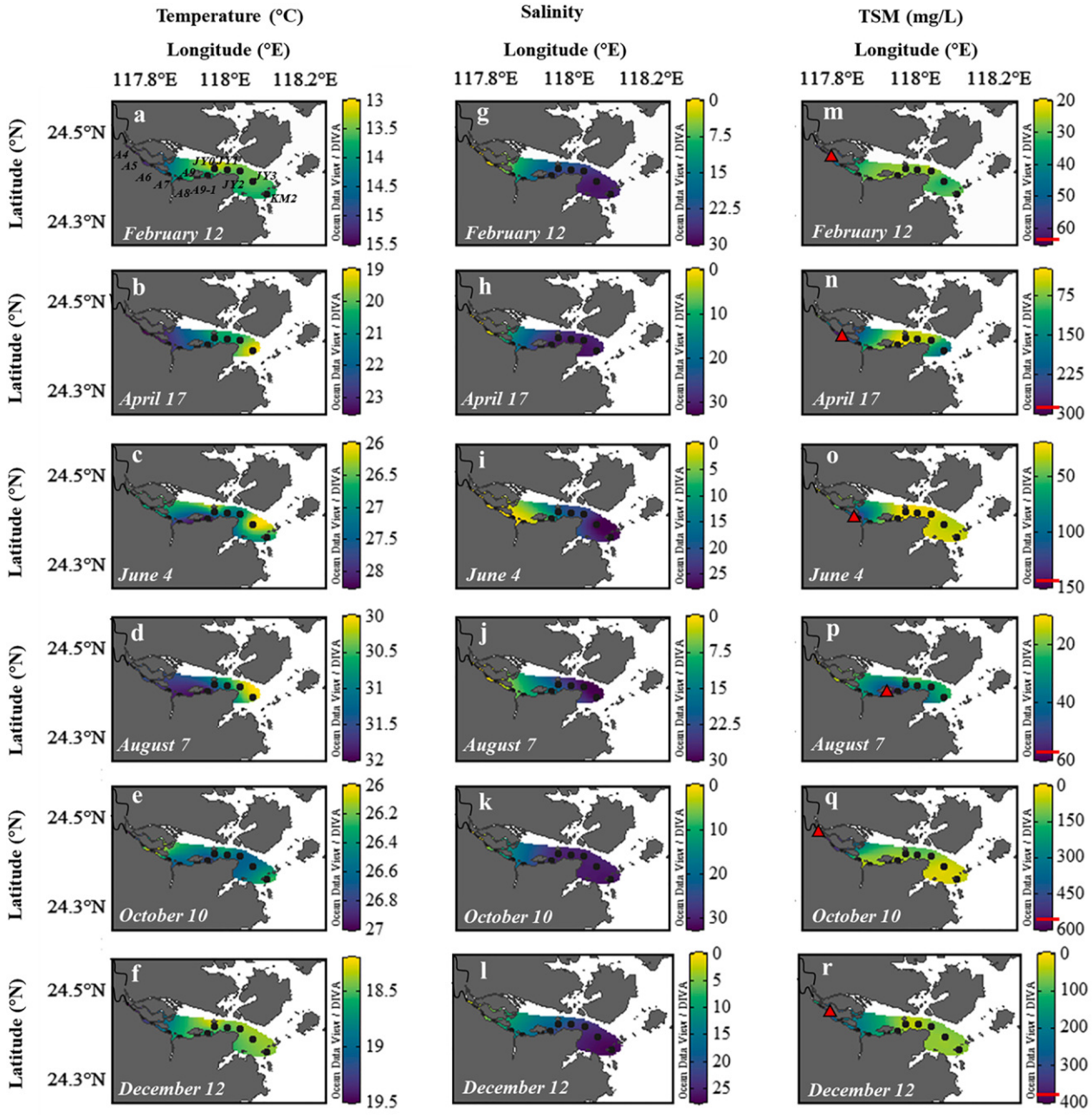

Fig. 3. Surface distributions of temperature (a-f), salinity (g-l), and TSM (m-r) along longitude in the Jiulong River estuary from February to December in 2014. The red triangles in m-r denote the location of TSM maxima and the corresponding value is marked in the colorbar with red dash.

while during the ebb tide

$$Corrected\ I(t) = I(t) - \left[h(t) - h(t-1) \times {}^{i}Ra_{total}(t)\right] \quad (6)$$

Next, the net Ra flux (F_{net}) over each measurement interval was estimated, $\Delta t = 1$ h,

$$F_{net} = [Corrected\ I(t) - Corrected\ I(t-1)]/\Delta t \quad (7)$$

The minimum mixing loss was estimated based on the maximum negative fluxes that were invariably present. The total Ra flux (F_{total}) was the sum of the net and the mixing flux (F_{mix}),

$$F_{total} = F_{net} + F_{mix} \quad (8)$$

Finally, the SGD rate (v) was calculated by dividing the Ra activity of the SGD endmember,

$$v = F_{total} / {}^{i}Ra_{SGD} \quad (9)$$

4. Results

4.1. Hydrological signature in the Jiulong River estuary

In 2014, the average ($n = 5$) temperature in the JRE, calculated from the measurements in the estuarine stations, ranged from 13.8 to 31.9 °C, with the highest in August and the lowest in February. During February, April, and December, the temperature generally decreased downstream, while in June, August, and October, localized maxima were observed in the mid estuary near the river mouth of the South Stream (Fig. 3a-f), which may result from the draining of the South Stream. The average ($n = 5$) salinity in the JRE ranged from 5.8 to 24.5 with April (24.5) > October (24.1) > February (17.1) > December (15.8) > August (9.8) > June (5.8). The spatial distribution of salinity followed a consistent pattern of increasing downstream along the main channel toward Xiamen Bay throughout the year without obvious influence from the South stream (Fig. 3g-l). Combining this with the river discharge data in Table 1, it is evident that the temporal pattern of salinity does not correspond well with river discharge, e.g., salinity peaked in April, while the river discharge was not the lowest during this period, suggesting that mixing in the estuary resulted not simply from the river and seawater, but with additional fresh water source.

The TSM concentration was up to 560 mg/L in December, while as low as 10.9 mg/L in August (Supporting Information Dataset 1), with an average ($n = 71$) of 92.2 mg/L in 2014. Along the main channel, the TSM concentration generally decreased downstream toward Xiamen bay, with the turbidity maximum zone (TMZ) appearing at different stations in different months (Fig. 3m-r). In February and April, TMZ appeared upstream with the maximum TSM of 62.0 and 294 mg/L, respectively, while in June and August, TSM had the maximum of 142 and 58.3 mg/L, respectively in the middle estuary. In October and December, TMZ migrated upstream with the maximum of 560 mg/L and 374 mg/L, respectively.

4.2. Spatial and temporal variations of long-lived radium isotopes in the JRE

The surface activities of ^{226}Ra and ^{228}Ra (dpm/100 L) showed a unimodal spatial pattern in the JRE, ranging from 12.0 ± 0.4 to 46.7 ± 0.8 and 21 ± 1 to 137 ± 2, respectively (Fig. 4). Their peaks were observed at mid salinity of 10 - 25. The maximum monthly average activity appeared in December, (32.1 ± 0.2) (dpm/100 L ($n = 12$) for ^{226}Ra and (104.1 ± 0.9) dpm/100 L ($n = 12$) for ^{228}Ra. The minimum monthly average ^{226}Ra, (28.3 ± 0.2) dpm/100 L ($n = 12$), appeared in October and ^{228}Ra as low as (61.5 ± 0.5) dpm/100 L was observed in August (Supporting Information Dataset 1).

During a diel cycle, the variations of ^{226}Ra and ^{228}Ra activities at Station A8 were in accordance with water depth and salinity (Fig. 5). The peaks of radium activity, (29.1 ± 0.8) dpm/100 L for ^{226}Ra and (94 ± 3) dpm/100 L for ^{228}Ra, showed up at the tidal crest, where the highest salinity was observed, while the lowest activities, (8.3 ± 0.2) dpm/100 L for ^{226}Ra and (18.1 ± 0.7) dpm/100 L for ^{228}Ra, appeared at the tidal trough where the lowest salinity was monitored (Supporting Information Dataset 3).

Table 1
Return flow factor (unitless), flushing time (day), river discharge (10^7 m^3/day), and SGD flux (10^7 m^3/day) calculated using ^{226}Ra and ^{228}Ra in 2014 with Low- and High- Salinity SGD endmembers.

Date	$b_^{226}$Ra		$b_^{228}$Ra		$T_f_^{226}$Ra		$T_f_^{228}$Ra		$F_{SGD}_^{226}$Ra		$F_{SGD}_^{228}$Ra		F_R	F_{SGD}/F_R
	LS	HS	LS	HS	LS	HS	LS	HS	LS	HS	LS	HS		average (n = 4)
12-Feb	0.66 (0.23)	0.66 (0.23)	0.66 (0.23)	0.65 (0.23)	2.52 (1.44)	2.52 (1.44)	2.52 (1.44)	2.50 (1.44)	0.27 (0.30)	0.27 (0.30)	0.23 (0.29)	0.24 (0.30)	3.67	6.88 %
17-Apr	0.81 (0.20)	0.81 (0.20)	0.80 (0.20)	0.80 (0.20)	4.48 (3.46)	4.49 (3.45)	4.46 (3.44)	4.42 (3.38)	−0.007 (0.25)	−0.007 (0.25)	0.11 (0.23)	0.11 (0.23)	4.3	1.12 %
4-Jun	0.24 (0.27)	0.2 4 (0.27)	0.24 (0.27)	0.24 (0.27)	1.10 (0.34)	1.10 (0.34)	1.10 (0.34)	1.10 (0.34)	1.11 (0.64)	1.1 (0.92)	0.7 (0.49)	0.7 (0.49)	6.56	13.80 %
7-Aug	0.35 (0.15)	0.35 (0.15)	0.35 (0.15)	0.35 (0.16)	1.03 (0.22)	1.03 (0.22)	1.03 (0.22)	1.02 (0.22)	0.92 (0.30)	0.92 (0.30)	0.68 (0.26)	0.69 (0.26)	3.8	21.12 %
10-Oct	0.77 (0.21)	0.77 (0.21)	0.77 (0.21)	0.77 (0.21)	4.26 (3.06)	4.24 (3.04)	4.25 (3.05)	4.19 (2.98)	0.03 (0.28)	0.03 (0.28)	0.2 (0.27)	0.21 (0.28)	3.61	3.30 %
12-Dec	0.58 (0.17)	0.59 (0.17)	0.58 (0.17)	0.58 (0.17)	1.90 (0.71)	1.92 (0.73)	1.90 (0.71)	1.89 (0.71)	0.47 (0.30)	0.45 (0.30)	0.49 (0.31)	0.5 (0.32)	2.89	16.52 %
4-Jan, 2011*	0.62 (0.28)	0.62 (0.28)	0.61 (0.29)	0.61 (0.29)	2.06 (1.35)	2.04 (1.32)	2.05 (1.34)	2.03 (1.31)	0.26	0.54	0.56	0.66	3.32	15.20 %
1-Apr, 2011*	0.61 (0.25)	0.61 (0.25)	0.61 (0.25)	0.61 (0.25)	2.34 (1.31)	2.37 (1.34)	2.36 (1.33)	2.33 (1.30)	0.29	0.6	0.57	0.67	3.36	15.90 %
5-Jul, 2010*	0.25 (0.31)	0.25 (0.31)	0.25 (0.31)	0.25 (0.31)	0.77 (0.27)	0.78 (0.27)	0.78 (0.27)	0.77 (0.27)	0.69	1.44	0.92	1.09	9.05	11.40 %
23-Nov, 2011*	0.44 (0.28)	0.44 (0.28)	0.44 (0.28)	0.44 (0.28)	2.02 (0.88)	2.03 (0.89)	2.03 (0.89)	2.03 (0.89)	0.45	0.93	0.59	0.69	4.97	13.40 %

Note: The numbers in parentheses represent errors. b denotes the fraction of ocean water, T_f denotes the flushing time, F_R denotes the river discharge. $F_{SGD}_^{i}$Ra ($i = 226$, 228) with LS denotes the flux of SGD calculated using ^{i}Ra of the low salinity (S = 6.5) SGD end member. $F_{SGD}_^{i}$Ra ($i = 226$, 228) with HS denotes the flux of SGD calculated using ^{i}Ra of the high salinity (S = 15) SGD end member. F_{SGD}/F_R average represents the ratio of the average flux of SGD to the river discharge. The sampling date marked with asterisk denote the data from Wang et al. (2015).

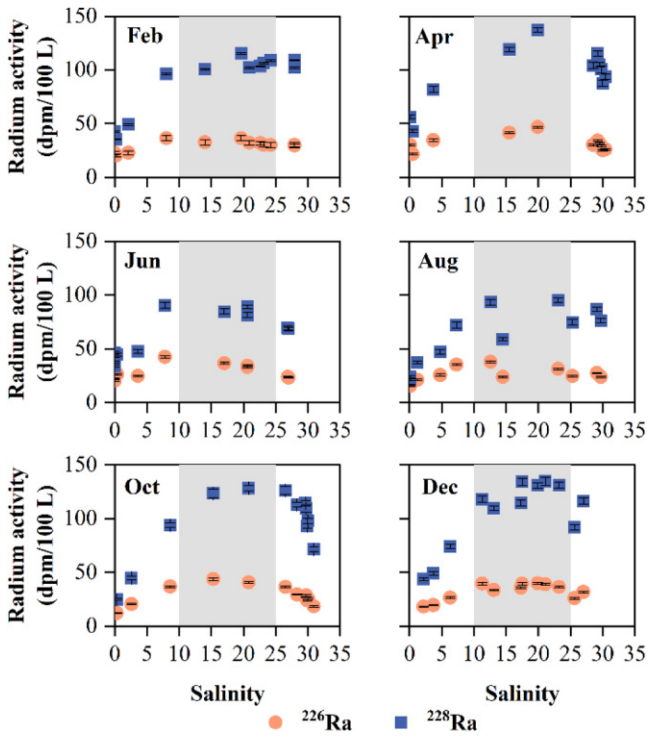

Fig. 4. Distributions of ^{226}Ra (a-f) and ^{228}Ra (g-l) along salinity in the JRE in 2014. The gray shading areas denote the salinity range from 10 to 25 (For interpretation of the references to color in this figure legend, the reader is referred to the web version of this article).

4.3. Flushing time in the JRE

The flushing time calculated using ^{226}Ra and ^{228}Ra show robustness with the two SGD end-members in the JRE (Table 1) and is significantly different between different months (One-sample T test, $p > 0.05$ (=0.998)). On average ($n = 4$), the intra-annual variation of flushing time is April (4.46 ± 1.72 day) > October (4.24 ± 1.52 day) > February (2.52 ± 0.72 day) > December (1.90 ± 0.36 day) > June (1.10 ± 0.17 day) > August (1.03 ± 0.11 day). The annual average flushing time in 2014 was (2.54 ± 0.41) days ($n = 24$).

4.4. The Flux of SGD in the JRE

Because of the non-point source character of SGD, it is challenging to determine the specific site where it flows into the surface estuary as well as the SGD end-member. In this study, we took the SGD end-member, one low salinity and one high salinity, to represent the mixture of seawater and groundwater in the aquifer (Wang et al., 2015) and to estimate the range of the flux of SGD. Additionally, to validate the reliability of the end-members, we conducted sensitivity analysis. The results indicate that the flux of SGD in the JRE is more sensitive to the change of radium activity in the end-members rather than salinity (see the Appendix A6). Considering that the spatial difference among different end-members are much greater than the temporal difference within each end-member, this suggests that our end-members are adequate for capturing the range of SGD flux.

During February to December in 2014, the flux of SGD shows great temporal fluctuations (Fig. 6), ranging from -0.007×10^7 to 1.10×10^7 m^3/day (Table 1). The flux reaches its maximum, 0.70×10^7 - 1.10×10^7 m^3/day, in June and its minimum, -0.007×10 - 0.11×10 m^3/day, in April. The ratio of the average flux of SGD in each sampling month ($n = 4$) to the concurrent river discharge ranges from 1.12 ± 2.79 % - 21.12 ± 3.68 % with the highest in August and the lowest in April. In addition, it is 13.80 ± 3.45 % in June and 16.52 ± 5.37 % in December, and decreases to 6.88 ± 4.04 % in February. The monthly average flux of SGD in 2014 falls in a range that encloses previous estimates in the JRE, $0.26 \times 10^7 - 1.09 \times 10$ m^3/day (Wang et al., 2015). Even with values different in the same month, the flux of SGD calculated with ^{226}Ra and ^{228}Ra presents consistent intra-annual and seasonal patterns, i.e., June > August > December > February > October > April. Furthermore, taking April as spring, June and August as summer, October as fall, and December as winter, the seasonal pattern of SGD flux in the JRE in 2014 is summer > winter > fall > spring. We calculated the average total SGD flux ($n = 4$) for each sampling month by using ^{226}Ra and ^{228}Ra, along with low and high salinity SGD endmembers. We then divided this by the surface area of the estuary, which is 7.11×10^7 m^2, to determine the SGD rate. Through such normalization to the sediment area of the estuary, the SGD rate in the JRE ranges from 0.007 ± 0.017 - 0.13 ± 0.04 m/day.

Applying the two isotope tracers with low- and high- salinity end-members, we also obtained the SGD seepage rate at the time-series station. On average at each sampling time ($n = 4$), the SGD seepage rate ranges from 0 - 3.39 m/day, with a total average of 1.27 ± 0.027 m/day ($n = 22$) (Fig. 5).

5. Discussion

5.1. Influencing factors of the flux of SGD in the Jiulong River estuary

Terrestrial factors such as precipitation, drainage geometry, and river discharge are demonstrated to affect the flow of fresh SGD remarkably (Diego-Feliu et al., 2022; Hsu et al., 2020). In addition, relatively high SGD flux in summer is proposed to be related to

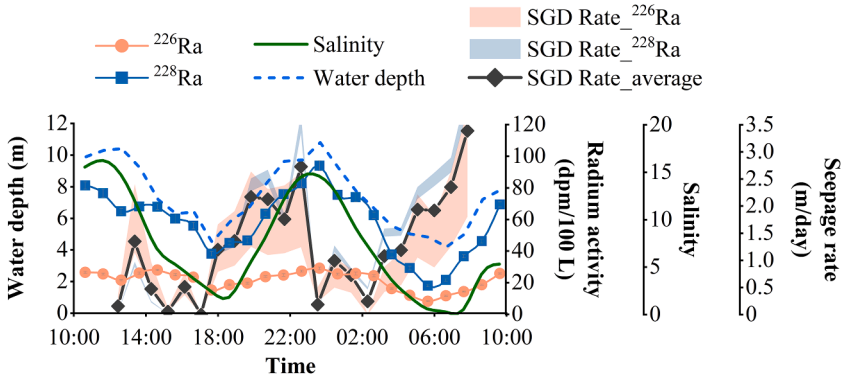

Fig. 5. Temporal variations of radium isotopes, water depth, salinity, and SGD rate at Station A8 over a diurnal cycle in the JRE. The color bands represent the range of SGD rate estimated with the low- and high- salinity end-members. The average SGD rate is based on all four results estimated using ^{226}Ra and ^{228}Ra with low- and high- salinity end-members.

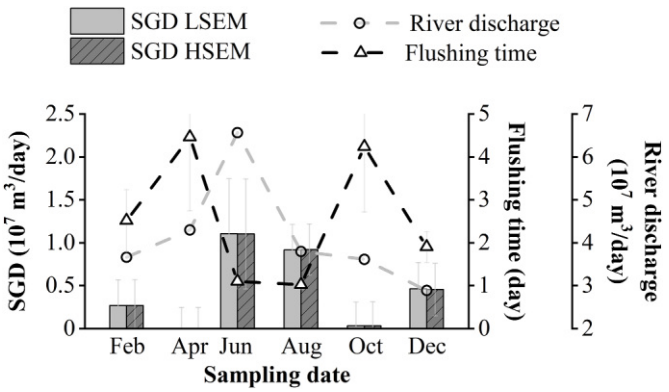

Fig. 6. The flux of SGD, river discharge, and flushing time in the JRE from February to December 2014. The river discharge is a weekly average prior to each investigation. 'LSEM' and 'HSEM' represent the average value (n = 2) of the flux of SGD traced with ^{226}Ra and ^{228}Ra calculated using the SGD Low and High Salinity End Member, respectively. The triangle denotes the average (n = 4) flushing time calculated every month. The light gray bar denotes the propagated error (For interpretation of the references to color in this figure legend, the reader is referred to the web version of this article).

groundwater elevation (Charette, 2007), river discharge (Sugimoto et al., 2016), or rainfall changes (Hougham et al., 2008). Tidal effects, such as tidal pumping or wave setup, are also considered to be the primary driven factors of SGD flux in some estuaries (Jiang et al., 2021; Robinson et al., 2018; Wang et al., 2014).

To evaluate the influence of hydrological factors on the flux of SGD in the JRE, we carried out PCA analysis of the bimonthly data. The results reveal a strong positive correlation between the SGD flux in the JRE and concurrent river discharge, as opposed to precipitation (Fig. 7). This suggests that the recharge of SGD may be not directly from precipitation, but more likely via the rivers. It is also likely that there is a time lag between the recharge from precipitation and groundwater table variation, which can not be resolved with PCA analysis. Time lag of months between rainfall and groundwater table is also reported based on long term observations (Zhang et al., 2017), which would weaken the correlation between SGD flux and rainfall. Moreover, the observation and numerical model results at Waquoit Bay show 1 – 5 months time lag between inland fresh recharge maximum and hydraulic head maximum (Michael et al., 2005). Thus, we infer that the SGD in the JRE sourced from shallow aquifers with more porous geological structure, which contribute a fast response of SGD to surface runoff generally.

Despite this, we observed that in April and October, although the river discharge during these periods is comparable to that in February, the SGD flux is notably smaller (Fig. 6). This discrepancy reflects the influence of hydrodynamics on the general pattern of surface runoff contributing to SGD. This indicates that the general pattern of surface runoff contributing to groundwater is influenced by hydrodynamics. The PCA results further reveal a significant negative correlation between SGD flux and flushing time, as well as return flow factor. In April and October, with higher return flow factor and longer estuarine water flushing time, these factors likely contribute to the observed lower SGD flux during these periods. Flushing time is an integrative parameter that describes the general exchange characteristics of water mass in a confined area without identifying the underlying processes such as river discharge, tidal mixing, and seawater dilution (Monsen et al., 2002). The larger return flow factor, associated with longer flushing time, indicates stronger exchange of the estuary water with the coastal water. During this period, the estuary water presents character of higher salinity, thus may cause smaller hydraulic gradient between submarine groundwater table and surface runoff table (Gonneea et al., 2013), which may lead to lower SGD flux in the JRE. Such extreme cases may occur in April, when the SGD flux was negative, implying intrusion of coastal saline water into the aquifer. Synoptically, the PCA results imply that when considering the estuary as a cohesive entity connecting the land and the ocean, disregarding the environmental gradients within the estuary, the terrestrial driving factors dominate the SGD flux in the JRE on a monthly scale.

On a timescale of days, the tidal effect on SGD in the JRE has not been revealed. Based on our time-series observations for 24 h with 1 h resolution at Station A8, the ^{226}Ra activity presents significant positive correlation with water depth during tidal cycles (Fig. 8a). Besides, the variation of water depth (4.2 - 10.8 m) during the diel cycle explained 69 % ($p < 0.001$) variations of ^{226}Ra activity (Fig. 8a). In addition, our cross correlation between ^{226}Ra activity and water depth demonstrates that the maximum cross correlation coefficient of 0.78 occurred at lag = 0 hour (Fig. 8b), implying a highly positive correlation between ^{226}Ra activity and water depth without hourly time lag. The surface sediments at Station A8 is mainly composed of coarse medium sands, which may contribute to a rapid positive response of groundwater signals to water depth. However, the SGD rate at the time-series station had no significant correlation with water depth and only 1.2 % of the variation of SGD rate can be explained by the water depth fluctuation (Fig. 8c). These results indicate

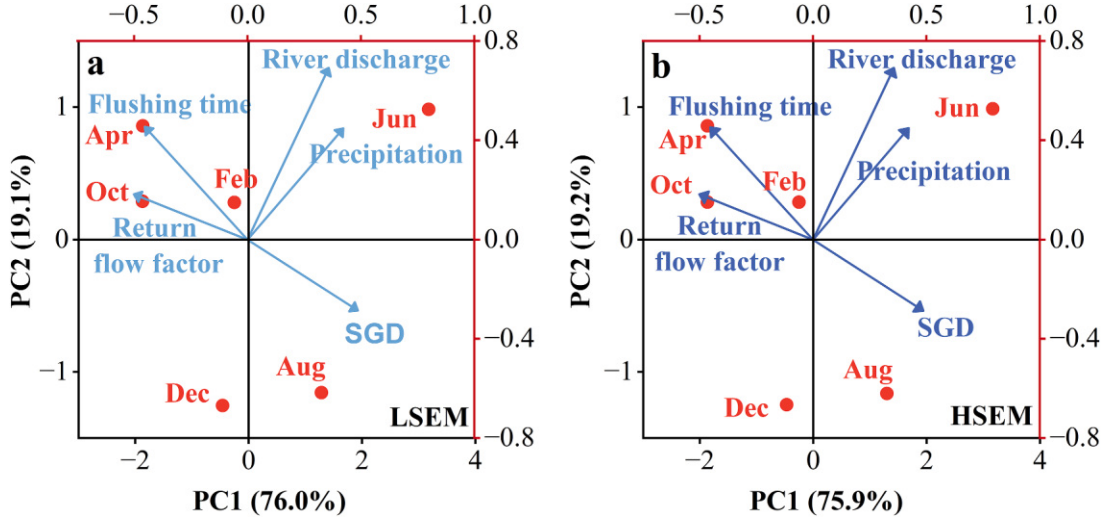

Fig. 7. PCA analysis of hydrological factors and SGD calculated using low- (a) and high- (b) salinity, respectively. Note that the SGD flux is the average (n = 2) value traced by ^{226}Ra and ^{228}Ra.

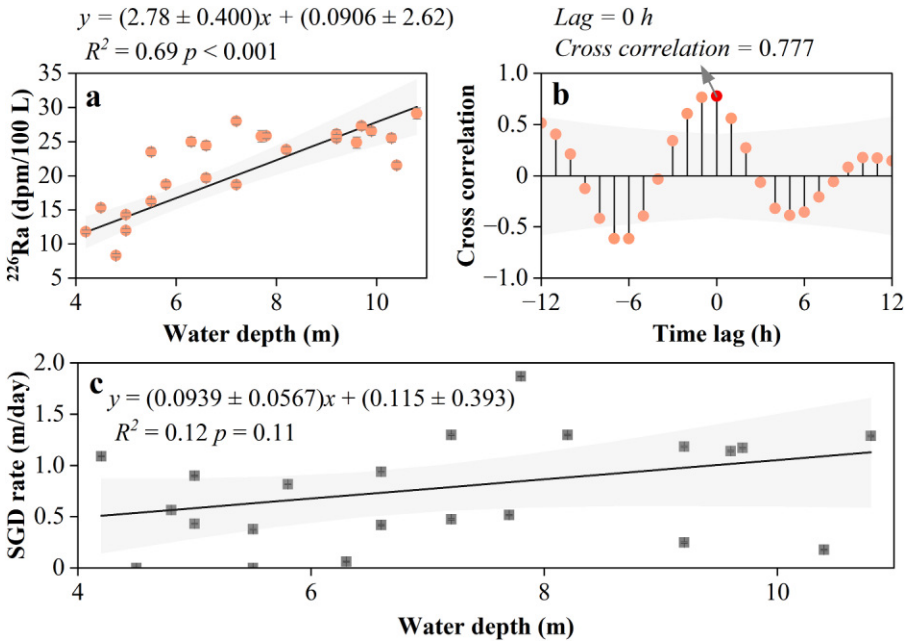

Fig. 8. The linear regression (a) and cross correlation (b) between radium activity and water depth. The linear regression between SGD rate and water depth (c). Note that all the results were based on ^{226}Ra as an example. Shading areas represent the 95 % confidence band. The red circle in panel b denotes the cross correlation at time lag = 0 h.

that tidal effect may not be the main driving force of SGD in the JRE. Station A8 is characterized by low to intermediate salinities of 0.3 – 16.3. In such a salinity range, the positive correlation between dissolved radium and water depth indicates that physical mixing predominated the radium behavior. During high tides, both water depth and salinity concurrently increased, with salinity reaching a maximum of 15 (Fig. 5). At such intermediate salinity levels, dissolved radium typically exhibited higher activities (Fig. 4). This phenomenon of peak activity of dissolved radium in estuaries within the intermediate salinity range has been observed in other studies as well. For example, in the Bega River estuary, the activity of radium reaches a maximum in the middle estuary with salinity of 14 – 20, and this is attributed to the extent and rate of leaching of the sediments (Hancock and Murray, 1996). Similarly, in the Pettaquamscutt estuary, the relative high activities of ^{226}Ra and ^{228}Ra are supposed to be a result of the desorption of surface-bound particulate radium (Kelly and Moran, 2002). However, due to the lack of in situ data on resuspended particles and total suspended particle concentrations at Station A8, further assessment is required to understand the impact of salinity-induced desorption signals from particles on the activity of dissolved radium in the water column in the JRE.

In numerous estuaries, researches consistently highlight the tidal pumping as a crucial driver of SGD. For example, the importance of tidal pumping as a driving force of SGD is revealed by significant negative correlations between radium activity and water depth in Sanya Bay (Wang et al., 2014). Other coastal regions such as in Kīholo Bay (McKenzie et al., 2021), annual observations with high temporal resolution of 1 h of the SGD rate and salinity reveal their negative correlation, which suggests that the tidal effect is the primary influencing factor of SGD. At Sanmen Bay, that SGD flux is negatively correlated with tidal height demonstrates the tidal pumping as a SGD driver (Liu et al., 2022). However, a limited number of studies with findings similar to our research in that tides seem not be the primary driving force of SGD have been reported.For example, the tidal pumping effect seems to be less important in a dry season along rocky-sandy shores (Kim and Hwang, 2002), which is revealed by the almost constant ^{222}Rn during the sampling period. Furthermore, the positive response of radium to water depth was also reported in the Da-Chia River estuary in a dry season (Hsu et al., 2020) and in a sandy aquifer at an estuarine transition zone at Tolo Harbor (Liu et al., 2018b). We thus infer that if the water table in the Jiulong River Basin is situated in geological layers with a relatively consistent hydraulic head, an increase in water depth will recharge the unconfined aquifer and lead to an increase in the SGD into the estuary.

5.2. *Proxies for the flux of SGD*

Considering the linear positive correlation between the flux of SGD and river discharge in 2014 in the JRE, as well as the negative correlations between the flux of SGD and flushing time and return flow factor (Fig. 7), we compiled historical and our data in the JRE to get an accessible proxy to serve model predictions of the flux of SGD and associated material fluxes. Our compilation indicates that the flux of SGD positively correlated with the river discharge in the JRE significantly (Fig. 9a). The slope of the regression indicates that the flux of SGD is equivalent to 13 % of the river discharge in the JRE (Fig. 9a). The negative intercept implies that SGD would be in a direction from the estuary into the coastal aquifer if the river discharge decreases to an extremely low value (Fig. 9a).

To investigate the factors leading to a positive response of the total SGD to the river discharge, we analyzed the recirculated and freshwater SGD components. The results show that RSGD, on average, constitutes approximately 44 – 100 % of the total SGD flux (Table A1). Notably, RSGD, with a substantial contribution to the overall SGD, presents positive response to the river discharge (Fig. A3a). The variation of RSGD would be equivalent to about 41% of the variation of river discharge, a value that is twice as much as the percentage for FSGD variations (Fig. A3). The noteworthy contribution of the RSGD to the overall SGD indicates that RSGD is the primary determinant for the observed positive response of the total SGD to river runoff. Despite the negative correlation between FSGD and river discharge (Fig. A3b), the limited proportion of FSGD in the total SGD in general with its contribution equivalent to RSGD only observed in October cannot alter the overall positive correlation between the total SGD and river discharge (Fig. 9a), which is primarily driven by the positive response of the RSGD to the river runoff.

Additionally, return flow factor and flushing time are highly negatively correlated with the flux of SGD in the JRE with $p < 0.0001$

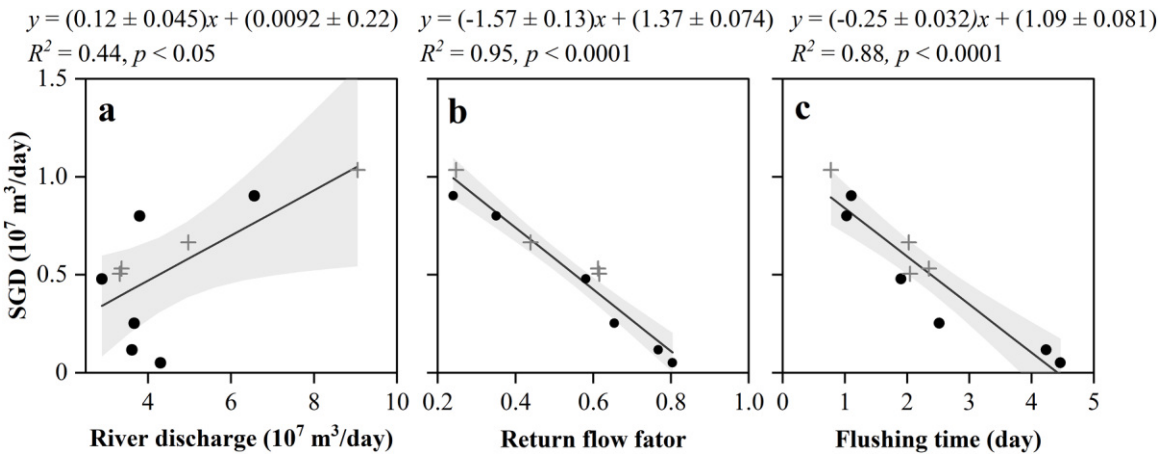

Fig. 9. Linear regression between the flux of SGD and river discharge (a), return flow factor (b) and flushing time (c). Shading area represents the 95 % confidence band. The regressions are all based on the compilation of this study (black circle) and Wang et al. (2015) (gray cross). Note that all the dots are the average ($n = 4$) of calculated results traced by ^{226}Ra and ^{228}Ra using low- and high-salinity SGD end-members (For interpretation of the references to color in this figure legend, the reader is referred to the web version of this article).

(Fig. 9b, c). The variation of return flow factor would explain 95 % variations of the SGD flux (Fig. 9b). Moreover, the negative correlation indicates that the smaller the fraction of ocean water retained in the estuary, indicating lower hydraulic pressure on the aquifer, the larger the SGD flux. The longest flushing time of 4.44 ± 2.38 days appears in April when the average salinity in the estuary is the highest and the flux of SGD is the minimum during the year. We infer that the sea water into the estuary remained relatively long in April so as to counteract the hydraulic pressure and recharge of surface water into the aquifer. The flushing time presents the largest difference of 77 ± 9.21 % between

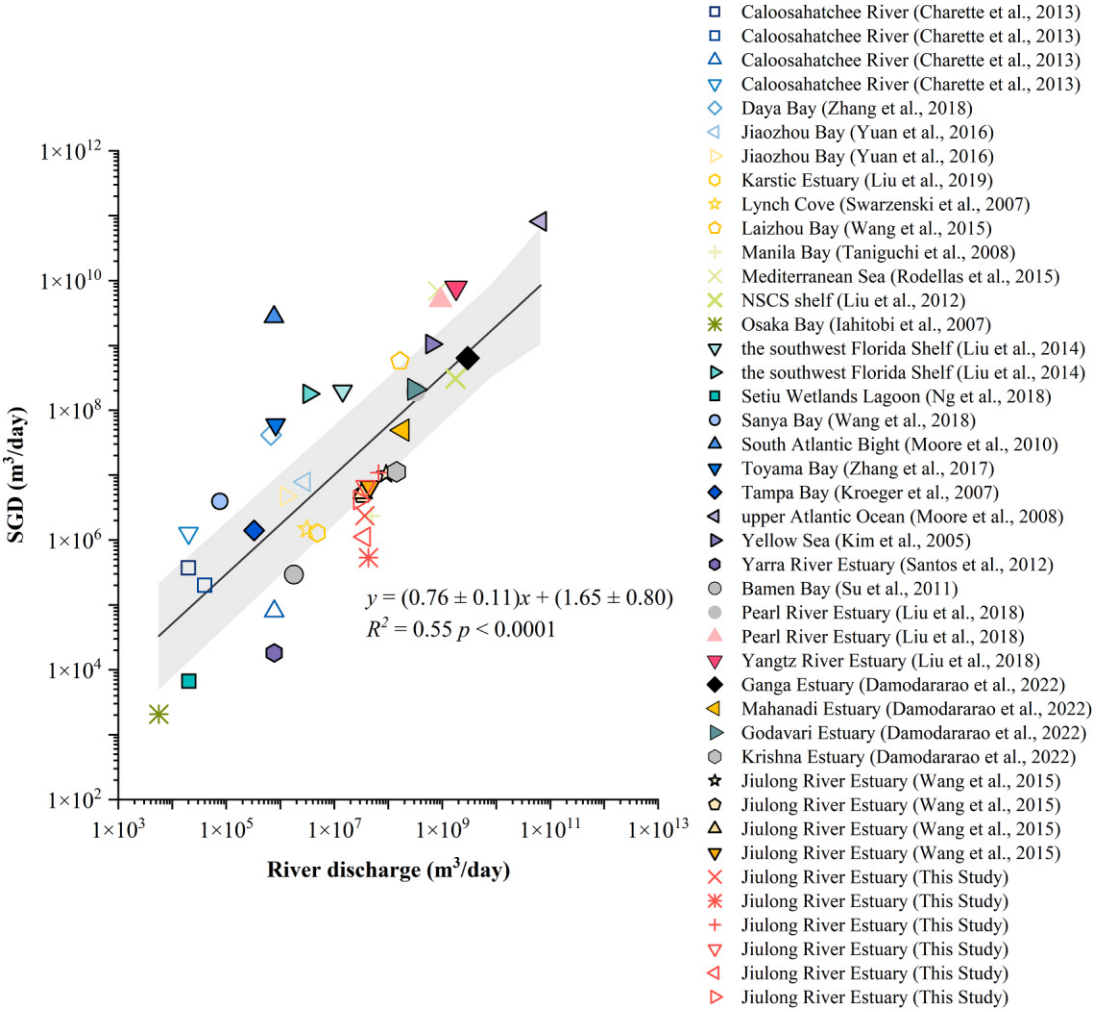

Fig. 10. The flux of SGD and river discharge in various systems. The solid line is the linear regression line and the shading area denote the 95 % confidence band.

April and August, even though the river discharges in these two months are similar (4.43×10^7 m^3/day in April and 3.80×10^7 m^3/day in August) with a difference of 11.7 %. This indicates that flushing time and return flow factor are indexes of the flux of SGD more sensitive than river discharge. Unfortunately, simultaneous estimations of the flux of SGD and flushing time in a global scale are so limited that a global compilation is not applicable.

5.3. Global perspectives

Considering that the data of river discharge are more accessible than return flow factor and flushing time, and to explore the relationship between the flux of SGD and river discharge on a global scale, we compiled SGD and contemporaneous river discharge in various systems around the globe with most of them estuaries (Supporting Information Dataset 4). The highest values were reported for the Upper Atlantic Ocean (Moore et al., 2008), while the lowest SGD flux and river runoff were observed in Osaka Bay (Ishitobi et al., 2007). Great spatiotemporal variations are present in the flux of SGD and river discharge with the highest and lowest SGD flux and concurrent river discharge differing by six orders of magnitude.

Considering such great variations, we took logarithmic scale of these compiled data in our statistical analysis to avoid an apparent linear correlation predominantly determined by the highest values that are at least three orders of magnitude greater than the others (Fig. A6). Interestingly, we found a significant positive correlation between the flux of SGD and river discharge for these systems ($R^2 = 0.55$, $p < 0.001$, Fig. 10). Based on the linear correlation in Fig. A6, the flux of SGD is predicted to be about 125 ± 2.0 % equivalent to the river discharge globally. This estimation overlaps with the result in the Atlantic Basin, where the flux of SGD was 0.8 - 1.6 times as much as the river flux (Moore et al., 2008).

Estuaries are hotspots of SGD due to their unique hydrogeological conditions and dynamic interactions between freshwater and seawater. Estuaries typically have highly permeable sediments that facilitate SGD and interaction of fresh groundwater and saline seawater in coastal aquifers. In such aquifers, remineralization of organic matter is so active that concentrations of chemical species, including biogenic elements carbon and nutrients, are highly enriched in SGD, which makes SGD a pathway as important as rivers in most estuaries (Ruiz-González et al., 2021; Slomp and Van Cappellen, 2004; Santos et al., 2021).

Although multiple driving factors may contribute to the heterogeneity of SGD in various systems in a global scale, including geological structures and tidal effects, our findings suggest that the flux of SGD is significantly related with river discharge globally, likely due to connectivity of coastal aquifer and rivers in estuaries. Notably, the fraction of FSGD is only nearly 1 % of the total fresh water input into the ocean and less than 1 % of the total SGD globally (Santos et al., 2021), yet the significant positive correlation between the flux of total SGD and river discharge seems to suggest a resonant relation between the total SGD (RSGD) and river discharge on a global scale. This resonance suggests that river discharge is also a potential proxy of the flux of SGD on a global scale, which may facilitate parameterization of SGD in coastal biogeochemical models and environmental assessments. The underlying mechanism for this resonance, however, awaits further exploration. Note the great regional variations in the flux of SGD and river discharge. When regional SGD comes under consideration, regional investigations and analysis may have to be carried out for a proper relationship applicable for a specific region.

6. Conclusions

We estimated the flux of SGD every other month in 2014 in the Jiulong River estuary with a three end-member mixing model and a long-lived Ra box model to explore potential hydrographic proxies of SGD. The flux of SGD (10^7 m^3/day) were estimated to range from 0.05 ± 0.12 in April to 0.90 ± 0.29 in June. A significant positive correlation was found between SGD flux and river discharge, likely due to connectivity between the coastal aquifer and the river. Furthermore, our time-series investigation in the mid estuary demonstrates that tidal pumping was not a major driving factor of the flux of SGD in the JRE based on positive responses of radium activities to the water depth. A significant negative correlation was found between the flux of SGD and flushing time as well as return flow factor. On a global scale, a significant positive correlation is present between the flux of SGD and river discharge in estuarine systems. Thus, we propose that three proxies of SGD, river discharge, return flow factor, and flushing time, be applicable in the JRE and river discharge be a global SGD proxy in model simulation and prediction.

CRediT authorship contribution statement

Moge Du: Writing – review & editing, Writing – original draft, Formal analysis, Data curation, Conceptualization. **Shilei Jin:** Validation, Methodology. **Siqi Wu:** Writing – review & editing. **Yanzhen Liao:** Data curation. **Guizhi Wang:** Writing – review & editing, Supervision, Resources, Methodology, Funding acquisition, Formal analysis, Conceptualization.

Declaration of competing interest

We declare that we have no financial and personal relationships with other people or organizations that can inappropriately influence our work, there is no professional or other personal interest of any nature or kind in any product, service and/or company that could be construed as influencing the position presented in, or the review of, the manuscript entitled.

Data availability

Data will be made available on request.

Acknowledgements

We thank the crew on R/V Ocean II for their assistance in the cruises. Ehui Tan, Liwen Chen, Zhangyong Wang, Qing Li, and Shengyao Sun helped in sample collection and measurements. Thanks for the precipitation data provided by the Data Center of National Observation and Research Station for the Taiwan Strait Marine Ecosystem (T-SMART) and Marine Monitoring & Information Service Center, Xiamen University (MMIS) and thanks are given to Shuiying Huang and Honghua Liu for help with data compiling. The cruises were supported by National Observation and Research Station for the Taiwan Strait Marine Ecosystem, Xiamen University. The research was supported by the National Natural Science Foundation of China (Project Number: 41576074), the Ministry of Science and Technology of China (Project Number: 2022YFC3105402), and partially supported by a grant from the Research Grants Council of the Hong Kong Special Administrative Region, China (Project Reference Number: AoE/P-601/23-N).

Supplementary materials

Supplementary material associated with this article can be found, in the online version, at doi:10.1016/j.watres.2024.121854.

References

Boehm, A.B., Paytan, A., Shellenbarger, G.G., Davis, K.A., 2006. Composition and flux of groundwater from a California beach aquifer: implications for nutrient supply to the surf zone. Cont. Shelf. Res. 26 (2), 269–282. https://doi.org/10.1016/j.csr.2005.11.008.

Burnett, W.C., Dulaiova, H., 2003. Estimating the dynamics of groundwater input into the coastal zone via continuous radon-222 measurements. J. Environ. Radioactiv. 69 (1), 21–35. https://doi.org/10.1016/S0265-931X(03)00084-5.
Burnett, W., Dulai, H., Stringer, C., Peterson, R., 2006. Submarine groundwater discharge: its measurement and influence on the coastal zone. J. Coastal Res. 35–38.
Charette, M.A., 2007. Hydrologic forcing of submarine groundwater discharge: insight from a seasonal study of radium isotopes in a groundwater-dominated salt marsh estuary. Limnol. Oceanogr. 52 (1), 230–239. https://doi.org/10.4319/lo.2007.52.1.0230.
Chen, B., Liu, H., Huang, B., Wang, J., 2014. Temperature effects on the growth rate of marine picoplankton. Mar. Ecol. Prog. Ser. 505, 37–47. https://doi.org/10.3354/meps10773.
Crusius, J., Koopmans, D., Bratton, J.F., Charette, M.A., Kroeger, K., Henderson, P., Ryckman, L., Halloran, K., Colman, J.A., 2005. Submarine groundwater discharge to a small estuary estimated from radon and salinity measurements and a box model. Biogeosciences 2 (2), 141–157.
Debnath, P., Mukherjee, A., 2016. Quantification of tidally-influenced seasonal groundwater discharge to the Bay of Bengal by seepage meter study. J. Hydrol. 537, 106–116. https://doi.org/10.1016/j.jhydrol.2016.03.010.
Diego-Feliu, M., Rodellas, V., Alorda-Kleinglass, A., Saaltink, M., Folch, A., Garcia-Orellana, J., 2022. Extreme precipitation events induce high fluxes of groundwater and associated nutrients to coastal ocean. Hydrol. Earth Syst. Sci. 26 (18), 4619–4635.
Duque, C., Michael, H.A., Wilson, A.M., 2020. The subterranean estuary: technical term, simple analogy, or source of confusion? Water Resour. Res. 56 (2), e2019WR026554 https://doi.org/10.1029/2019WR026554.
Escobar Correa, R., 2021. Submarine Groundwater Discharge Estimated from Isotopic Tracers : Implications to Carbon Cycling in Three Coastal Systems. Southern Cross University, p. 112. https://doi.org/10.25918/thesis.154.
Gonneea, M.E., Mulligan, A.E., Charette, M.A., 2013. Climate-driven sea level anomalies modulate coastal groundwater dynamics and discharge. Geophys. Res. Lett. 40 (11), 2701–2706. https://doi.org/10.1002/grl.50192.
Goodridge, B.M., 2018. The influence of submarine groundwater discharge on nearshore marine dissolved organic carbon reactivity, concentration dynamics, and offshore export. Geochim. Cosmochim. Ac. 241, 108–119. https://doi.org/10.1016/j.gca.2018.08.040.
Hancock, G., Murray, A., 1996. Source and distribution of dissolved radium in the Bega River estuary, Southeastern Australia. Earth Planet. Sci. Lett. 138 (1–4), 145–155.
Hougham, A.L., Moran, S.B., Masterson, J.P., Kelly, R.P., 2008. Seasonal changes in submarine groundwater discharge to coastal salt ponds estimated using 226Ra and 228Ra as tracers. Mar. Chem. 109 (3), 268–278. https://doi.org/10.1016/j.marchem.2007.08.001.
Hsu, F.-H., Su, C.-C., Wang, P.-L., Lin, I.-T., 2020. Temporal variations of submarine groundwater discharge into a tide-dominated coastal wetland (Gaomei Wetland, Western Taiwan) indicated by radon and radium isotopes. Water. 12 (6), 1806. https://doi.org/10.3390/w12061806.
Ishitobi, T., Taniguchi, M., Umezawa, Y., Kasahara, S., Onodera, S.-I., Hayashi, M., Miyaoka, K., 2007. Investigation of submarine groundwater discharge using several methods in the inter-tidal zone. IAHS-AISH Publication 60–67.
Jiang, Y.W., Wai, O.W.H., 2005. Drying–wetting approach for 3D finite element sigma coordinate model for estuaries with large tidal flats. Adv. Water. Resour. 28 (8), 779–792. https://doi.org/10.1016/j.advwatres.2005.02.004.
Jiang, Z.-P., Lv, J., Li, Q., Dai, M., Kao, S.-J., Zheng, N., Fan, W., 2021. Tidal-driven submarine groundwater discharge and its influences on the carbonate system of a coastal coral reef in the northern South China Sea. J. Geophys. Res.-Oceans 126 (7), e2021JC017203.
Kelly, R., Moran, S., 2002. Seasonal changes in groundwater input to a well-mixed estuary estimated using radium isotopes and implications for coastal nutrient budgets. Limnol. Oceanogr. 47 (6), 1796–1807.
Kim, G., Hwang, D.-W., 2002. Tidal pumping of groundwater into the coastal ocean revealed from submarine 222Rn and CH4 monitoring. Geophys. Res. Lett. 29 (14), 23. https://doi.org/10.1029/2002GL015093.
Kim, G., Lee, K.-K., Park, K.-S., Hwang, D.-W., Yang, H.-S., 2003. Large submarine groundwater discharge (SGD) from a volcanic island. Geophys. Res. Lett. 30 (21), 267–283. https://doi.org/10.1029/2003GL018378.
Kim, G., Ryu, J.-W., Hwang, D.-W., 2008. Radium tracing of submarine groundwater discharge (SGD) and associated nutrient fluxes in a highly-permeable bed coastal zone. Korea Mar. Chem. 109 (3), 307–317. https://doi.org/10.1016/j.marchem.2007.07.002.
Kwon, E.Y., Kim, G., Primeau, F., Moore, W.S., Cho, H.-M., DeVries, T., Sarmiento, J.L., Charette, M.A., Cho, Y.-K., 2014. Global estimate of submarine groundwater discharge based on an observationally constrained radium isotope model. Geophys. Res. Lett. 41 (23), 8438–8444.
Liu, Y., Jiao, J.J., Liang, W., Luo, X., 2018. Using tidal fluctuation-induced dynamics of radium isotopes (224Ra, 223Ra, and 228Ra) to trace the hydrodynamics and geochemical reactions in a coastal groundwater mixing zone. Water Resour. Res. 54 (4), 2909–2930. https://doi.org/10.1002/2017WR022456.
Liu, J., Yu, X., Du, J., 2022. Tidally driven submarine groundwater discharge to a marine aquaculture embayment: insights from radium and dissolved silicon. Mar. Pollut. Bull. 178, 113620 https://doi.org/10.1016/j.marpolbul.2022.113620.
Luijendijk, E., Gleeson, T., Moosdorf, N., 2020. Fresh groundwater discharge insignificant for the world's oceans but important for coastal ecosystems. Nat. Commun. 11 (1), 1260. https://doi.org/10.1038/s41467-020-15064-8.
McKenzie, T., Dulai, H., Fuleky, P., 2021. Traditional and novel time-series approaches reveal submarine groundwater discharge dynamics under baseline and extreme event conditions. Sci. Rep. 11 (1), 22570. https://doi.org/10.1038/s41598-021-01920-0.
Michael, H.A., Mulligan, A.E., Harvey, C.F., 2005. Seasonal oscillations in water exchange between aquifers and the coastal ocean. Nature 436 (7054), 1145–1148. https://doi.org/10.1038/nature03935.
Michael, H.A., Russoniello, C.J., Byron, L.A., 2013. Global assessment of vulnerability to sea-level rise in topography-limited and recharge-limited coastal groundwater systems. Water Resour. Res. 49 (4), 2228–2240. https://doi.org/10.1002/wrcr.20213.
Monsen, N.E., Cloern, J.E., Lucas, L.V., Monismith, S.G., 2002. A comment on the use of flushing time, residence time, and age as transport time scales. Limnol. Oceanogr. 47 (5), 1545–1553. https://doi.org/10.4319/lo.2002.47.5.1545.
Moore, W.S., Sarmiento, J.L., Key, R.M., 2008. Submarine groundwater discharge revealed by 228Ra distribution in the upper Atlantic Ocean. Nat. Geosci. 1 (5), 309–311. https://doi.org/10.1038/ngeo183.
Moore, W.S., 1999. The subterranean estuary: a reaction zone of ground water and sea water. Mar. Chem. 65 (1), 111–125. https://doi.org/10.1016/S0304-4203(99)00014-6.
Moore, W.S., 2003. Sources and fluxes of submarine groundwater discharge delineated by radium isotopes. Biogeochemistry 66 (1), 75–93. https://doi.org/10.1023/B:BIOG.0000006065.77764.a0.
Moore, W.S., 2006. Radium isotopes as tracers of submarine groundwater discharge in Sicily. Cont. Shelf Res. 26 (7), 852–861. https://doi.org/10.1016/j.csr.2005.12.004.
Robinson, C.E., Xin, P., Santos, I.R., Charette, M.A., Li, L., Barry, D.A., 2018. Groundwater dynamics in subterranean estuaries of coastal unconfined aquifers: Controls on submarine groundwater discharge and chemical inputs to the ocean. Adv. Water Resour. 115, 315–331.
Rodellas, V., Garcia-Orellana, J., Trezzi, G., Masqué, P., Stieglitz, T.C., Bokuniewicz, H., Cochran, J.K., Berdalet, E., 2017. Using the radium quartet to quantify submarine groundwater discharge and porewater exchange. Geochim. Cosmochim. Acta 196, 58–73.
Ruiz-González, C., Rodellas, V., Garcia-Orellana, J., 2021. The microbial dimension of submarine groundwater discharge: current challenges and future directions. Fems Microbiol. Rev. 45 (5) https://doi.org/10.1093/femsre/fuab010.
Sanford, L.P., Boicourt, W.C., Rives, S.R., 1992. Model for estimating tidal flushing of small Embayments. J. Waterway, Port, Coast. Ocean Eng. 118 (6), 635–654. https://doi.org/10.1061/(ASCE)0733-950X(1992)118:6(635).
Santos, I.R., Burnett, W.C., Dittmar, T., Suryaputra, I.G.N.A., Chanton, J., 2009. Tidal pumping drives nutrient and dissolved organic matter dynamics in a Gulf of Mexico subterranean estuary. Geochim. Cosmochim. Acta 73 (5), 1325–1339. https://doi.org/10.1016/j.gca.2008.11.029.
Santos, I.R., Eyre, B.D., Huettel, M., 2012. The driving forces of porewater and groundwater flow in permeable coastal sediments: a review. Estuar. Coast. Shelf Sci. 98 (12), 1–15. https://doi.org/10.1016/j.ecss.2011.10.024.
Santos, I.R., Chen, X., Lecher, A.L., Sawyer, A.H., Moosdorf, N., Rodellas, V., Tamborski, J., Cho, H.-M., Dimova, N., Sugimoto, R., Bonaglia, S., Li, H., Hajati, M.-C., Li, L., 2021. Submarine groundwater discharge impacts on coastal nutrient biogeochemistry. Nat. Rev. Earth Environ. 2 (5), 307–323.
Slomp, C.P., Van Cappellen, P., 2004. Nutrient inputs to the coastal ocean through submarine groundwater discharge: controls and potential impact. J. Hydrol. 295 (1), 64–86. https://doi.org/10.1016/j.jhydrol.2004.02.018.
Sugimoto, R., Honda, H., Kobayashi, S., Takao, Y., Tahara, D., Tominaga, O., Taniguchi, M., 2016. Seasonal Changes in Submarine Groundwater Discharge and Associated Nutrient Transport into a Tideless Semi-enclosed Embayment (Obama Bay, Japan). Estuaries Coasts 39 (1), 13–26.
Wang, G., Jing, W., Wang, S., Xu, Y., Wang, Z., Zhang, Z., Li, Q., Dai, M., 2014. Coastal acidification induced by tidal-driven submarine groundwater discharge in a coastal coral reef system. Environ. Sci. Technol. 48 (22), 13069–13075.
Wang, G., Wang, Z., Zhai, W., Moore, W.S., Li, Q., Yan, X., Qi, D., Jiang, Y., 2015. Net subterranean estuarine export fluxes of dissolved inorganic C, N, P, Si, and total alkalinity into the Jiulong River estuary, China. Geochim. Cosmochim. Acta. 149, 103–114.
Wang, X., Zhang, Y., Zheng, C., Luo, M., Yu, S., Lu, M., Li, H., 2021. Submarine Groundwater and River Discharges Affect Carbon Cycle in a Highly Urbanized and River-Dominated Coastal Area. Front. Mar. Sci. 8 https://doi.org/10.3389/fmars.2021.817001.
Yu, J., Tian, Y., Wang, X., Wang, X., Lancia, M., Li, H., Andrews, C.B., Zheng, C., 2022. A New Simulation-Optimization Framework for Estimation of Submarine Groundwater Discharge Based on Hydrodynamic Modeling and Isotopic Data. Geophys. Res. Lett. 49 (23), e2022GL098893.
Zhang, M., Krom, M.D., Lin, J., Cheng, P., Chen, N., 2022. Effects of a storm on the transformation and export of phosphorus through a subtropical river-turbid estuary continuum revealed by continuous observation. J. Geophys. Res. 127, e2022JG006786 https://doi.org/10.1029/2022JG006786.
Zhang, X., et al., 2024. A comprehensive analysis of submarine groundwater discharge and nutrient fluxes in the Bohai Sea, China. Water Resour. 253, 121320. https://doi.org/10.1016/j.watres.2024.121320.
Zhang, B., Zhang, J., Yoshida, T., 2017. Temporal variations of groundwater tables and implications for submarine groundwater discharge: a 3-decade case study in central Japan. Hydrol. Earth Syst. Sci. 21 (7), 3417–3425. https://doi.org/10.5194/hess-21-3417-2017.
Zuo, S., Han, Z., Huang, Y., Han, J., Xie, M.J.A.O.S., 2016. Distributions of surficial sediments and its response to dynamic actions in the Xiamen Bay sea area, China. Acta Oceanol. Sin. 35 (4), 9–18. https://doi.org/10.1007/s13131-016-0840-y.